Nonlinear site effects on strong ground motion at a reclaimed island

Jun Yang, Tadanobu Sato, and Xiang-Song Li

Abstract: Recently there has been an increased interest in the study of the nonlinearity in soil response for large strains through in situ earthquake observations. In this paper, the downhole array acceleration data recorded at a reclaimed island, Kobe, during the 1995 Kobe earthquake are used to study nonlinear site effects. Particular attention is given to the liquefaction-induced nonlinear effects on the recorded ground motions. By using the spectral ratio and the spectral-smoothing technique, the characteristics of the ground motions are analyzed. It is shown that the peak frequencies in spectral ratios were shifted to lower frequencies when the strongest motions occurred. The increase in the predominant period was caused primarily by a strong attenuation of low-period waves, rather than by amplification of long-period motions. Based on the spectral analyses, the nonlinearity occurring in the shallow liquefied layer during the shaking event is identified, manifested by a significant reduction of the shear modulus. A fully coupled, inelastic, finite element analysis of the response of the array site is carried out. The stress–strain histories of soils and excess pore-water pressures at different depths are calculated. It is suggested that the stress–strain response and the build up of pore pressure are well correlated to the variation of the characteristics of ground motions during the shaking history.

Key words: site response, ground motion, nonlinearity, soil liquefaction, array records, Kobe earthquake.

Résumé : Il y a eu récemment un intérêt accru pour l'étude de la non linéarité dans les réponses du sol pour les grandes déformations par le biais des observations in situ des tremblement de terre. Dans cet article, les données de réseau d'accélération en bout de forage enregistrées sur un île remblayée, Kobe, durant le séisme de Kobe en 1995 sont utilisées pour étudier les effets de site non linéaires. Une attention particulière a été apportée aux effets non linéaires sur les mouvements enregistrés du sol induits par la liquéfaction. En utilisant le rapport spectral de même que la technique de lissage spectral, les caractéristiques des mouvements du sol sont analysées. Il est montré que les fréquences de pic dans les rapports spectraux ont été déplacés vers des fréquences plus basses lorsque les mouvements les plus forts se produisaient. L'accroissement de la période prédominante a été causé principalement par la forte atténuation des ondes de faible période plutôt que par l'amplification des mouvements de grande période. D'après les analyses spectrales, la non linéarité se produisant dans la couche liquéfiée peu profonde durant les secousses a été identifiée et se manifestait par une réduction significative du module de cisaillement. L'on a effectué une analyse inélastique complètement couplée par éléments finis de la réponse du site du réseau. Les histoires de contrainte–déformation des sols et l'excédent des pressions interstitielles à différentes profondeurs ont été calculés. L'on aborde le fait que la réponse contrainte–déformation et le développement de la pression interstitielle sont en bonne corrélation avec la variation des caractéristiques des mouvements du sol durant l'histoire des secousses.

Mots clés : réponse du site, mouvement du sol, non linéarité, liquéfaction du sol, données de réseau, séisme de Kobe.

[Traduit par la Rédaction]

Introduction

It is well known that seismic amplification basically originates from the strong contrast between the physical properties of the sedimentary soils and the bedrock. Local soil conditions have a significant effect on the amplitude and frequency content of earthquake motions. Numerous laboratory tests have been done to investigate dynamic soil behavior over a wide range of strain (e.g., Seed and Idriss 1970; Hardin and Drnevich 1972; Kokusho 1980; Vucetic and Dobry 1991). Based on the laboratory findings, it is recognized that, if the earthquake shaking is strong enough to cause large strain above a certain threshold of a soil, the soil will respond nonlinearly, manifested by the shear modulus and damping ratio which vary with the amplitude of shear strain. In addition to the strain-dependent behavior in general, for saturated cohesionless soils subjected to undrained cyclic loading, the gradual buildup of excess pore-water pressure can reduce effective stresses and, consequently, the soil stiffness. This nonlinear effect induced by the accumulation of pore-water pressure is more complex when the pore-water pressure is high enough to bring soils to the state of liquefaction. Much work has been carried out to understand soil liquefaction (e.g., Seed 1979; NRC 1985; Ishihara 1993). Many constitutive equations based on laboratory test results have been developed for modeling soil nonlinearity

Received January 4, 1999. Accepted August 4, 1999.

J. Yang[1] and T. Sato. Disaster Prevention Research Institute, Kyoto University, Kyoto 611-0011, Japan.
X.-S. Li. Department of Civil Engineering, Hong Kong University of Science and Technology, Hong Kong, China.

[1]Author to whom all correspondence should be addressed.

and liquefaction. However, there is a concern that the laboratory conditions are not the same as those in the field. It is of importance, therefore, to study the nonlinearity in soil response for large strains through in situ earthquake observations. Such study is also helpful in verifying and refining the available laboratory observations and analytical simulations on soil behavior and ground response.

For a site subjected to earthquake shaking, in addition to the local soil conditions, whether nonlinear effects can occur or not depends on many other factors, such as the intensity of earthquake shaking (weak, moderate, or strong), the distance of the site from the source, and the subsurface topography. A most desirable way to accurately investigate the nonlinear response is through in situ observations obtained from vertical arrays in strong earthquakes. These array records make it possible to separate the local soil effects from source and path effects. One can investigate the nonlinear soil response by examining the Fourier spectral ratio between ground surface and bedrock motions. It is expected that the nonlinear effects are expressed in the reduction in the amplitude and the lengthening in the predominant period of surface ground motion. These may be two obvious features of nonlinear soil response which can be demonstrated by using the earthquake records. It is also possible to use these records to investigate the behavior of soils between the stations at different depths and how much this behavior influences the ground motion. However, one problem encountered in doing so is the scarcity of time history records in strong earthquakes which may show the characteristics of nonlinear effects. Recently, some researchers have tried to find observational evidence of the nonlinear site effects from earthquake motion data (Sugito and Kamada 1990; Chang et al. 1991; Beresnev et al. 1995; Elgamal et al. 1995). These works have resulted in an increased interest in the importance of nonlinear soil behavior and ground response recorded during earthquakes.

The objective of this paper is to study nonlinear effects using the vertical array strong motion records obtained at the reclaimed Port Island, Kobe, during the 1995 Kobe earthquake, with particular attention given to the effects of soil liquefaction on the characteristics of ground motions. The unique features of the Port Island records are as follows: (1) the records included detailed acceleration data at reasonably spaced depth intervals; the maximum recorded acceleration reached approximately 0.6*g* and the deepest accelerometer was located at a depth of 83 m; and (2) the site consisted of a reclaimed loose surface layer which liquefied during shaking events; abundant evidence of site liquefaction such as sand ejection, ground fissures, and lateral spreading of as much as 5.9 m was observed after the earthquake. Therefore, it is believed that the nonlinear soil response was triggered and its effects would be shown by these acceleration records. In this study, the characteristics of the recorded ground motions are analyzed using the spectral ratio and the spectral-smoothing technique. Based on the spectral analyses, the nonlinearity occurring in the shallow liquefied layer during shaking events is identified. Furthermore, a fully coupled, inelastic, finite element analysis is carried out to analyze the ground response at the array site. The stress–strain histories of soils and excess pore-water pressures at different depths are simulated and, in particular, their relations to the characteristics of the ground motions are addressed.

Fig. 1. Location of Port Island and the vertical array.

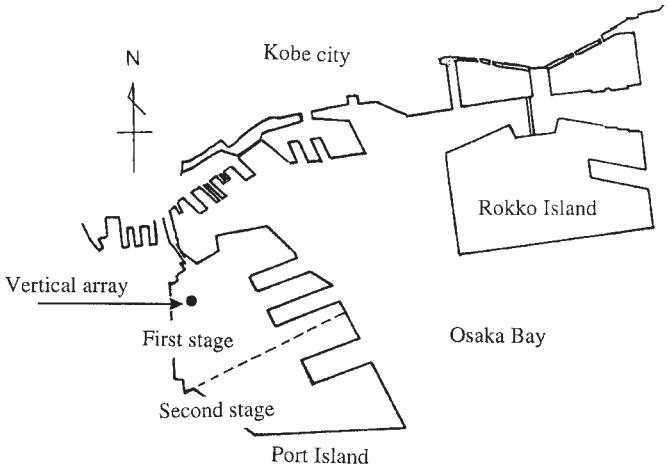

Site conditions and downhole array records

Port Island is an artificial island located on the southwest side of Kobe, Japan. The island was constructed in two stages. In the first stage, between 1966 and 1981, an area of 436 ha was reclaimed. In the second stage, which was started in 1986, the island was extended southward by reclaiming an area of 319 ha. A downhole array was installed at the northwest corner of Port Island in August 1991. The location of the island and the array site are shown in Fig. 1. The array consisted of three-component accelerometers located at the surface and at depths of 16, 32, and 83 m. All instruments were linked to a common triggering mechanism to record the seismic data synchronously. The downhole array site basically consisted of (1) a reclaimed surface layer down to a depth of 19 m which consisted of decomposed granite mined from nearby mountains; (2) an alluvial silty clay layer from a depth of 19–27 m; (3) alluvial sand between 27 and 33 m; (4) sand with gravel and diluvial sand from 33 to 61 m; (5) a diluvial silty clay layer between 61 and 79 m; and (6) sand with gravel below 79 m. The groundwater level was located at a depth of 2.4 m before the earthquake and it dropped to 3.5 m after the shaking events. Figure 2 shows the soil profile at the array site. The site investigation indicated that the standard penetration test (SPT) values of the surface reclaimed layer were very low, indicating that there existed a high liquefaction susceptibility in that layer. The grain sizes of soils used for the surface reclamation ranged from gravel- and cobble-sized particles to fine sands. Figure 3 shows the strain-dependent modulus reduction and damping ratio curves obtained from laboratory tests for the reclaimed soil, alluvial clay, and alluvial sand at the site (Kobe City Development Bureau 1995).

Strong motions in three components were recorded by the downhole array during the 1995 Kobe earthquake (Japan Meteorological Agency magnitude scale M_j = 7.2, roughly equivalent to a moment magnitude M_w = 6.9), as shown in Fig. 4. The peak accelerations were recorded as 527 gal (1 gal = 1 cm/s^2) (0.538*g*), 486 gal (0.496*g*), and 186 gal

Fig. 2. Soil profile at the vertical array site, Port Island.

Depth	Soil Type	Soil Description	Accelero-meter	P wave (m/s)	S wave (m/s)	SPT (N value)
0.0 m		Sandy gravel	0 m	260	170	5.2
2.0				330	170	5.2
5.0				780	210	6.5
12.6		Sand with gravel	16 m	1480	210	6.5
19.0		Alluvial clay		1180	180	3.5
27.0		Alluvial sand		1330	245	13.5
33.0		Sand with gravel	32 m	1530	305	36.5
50.0		Diluvial sand		1610	350	61.9
61.0		Diluvial clay		1610	303	11.7
79.0		Sand with gravel	83 m	2000	320	61.9
83.0						

Fig. 3. Modulus reduction and damping ratio curves for several types of soils at the array site.

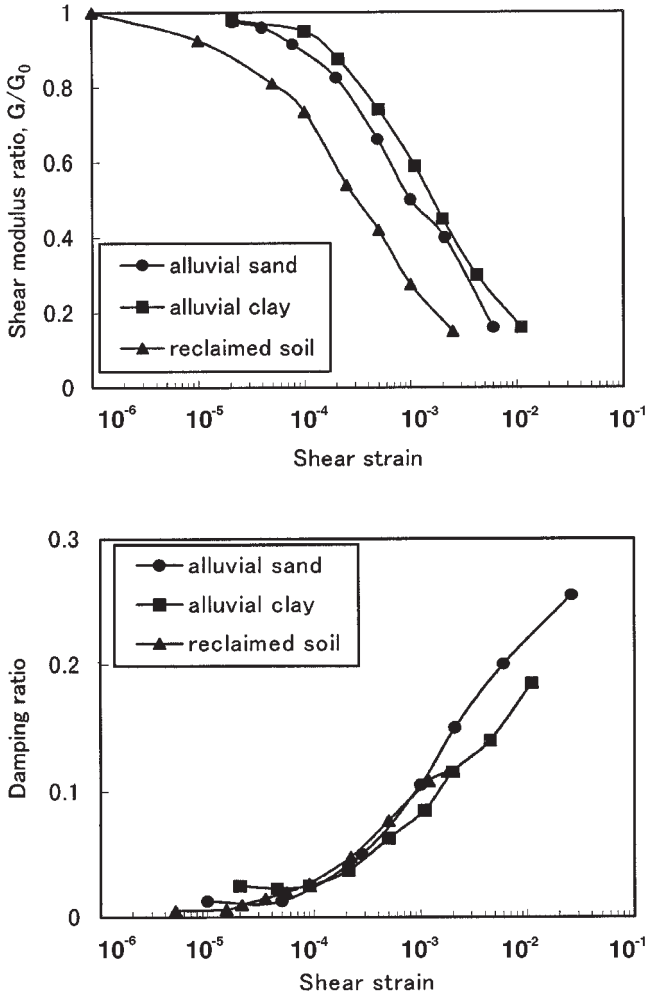

(0.190*g*) at a depth of 83 m (G.L. –83 m, where G.L. denotes ground level) for the north–south (NS), east–west (EW), and up–down (UD) components, respectively. It should be mentioned that the orientation error in the accelerometer at G.L. –83 m has been corrected according to the displacement orbits for each station in the horizontal plane (Sugito et al. 1996). The corrected displacement orbits at four stations at different depths are shown in Fig. 5. Moreover, it is to be noted that the acceleration records at G.L. –16 m in the vertical component contained some unusual impulse-like spikes; it is very probable that during strong motion the sensor malfunctioned, therefore the records in the vertical component at this depth are not used here. Figure 6 depicts the distribution of peak accelerations in three components with depth. A significant reduction of the amplitudes of horizontal motions took place when the seismic waves travelled from the bottom to the surface. On the other hand, the vertical motion was greatly amplified at the surface. To show the change of the relationship among the three components of the motions, the peak vertical accelerations are plotted against the peak horizontal accelerations in east–west and north–south directions at three different depths in Fig. 7, where two straight lines correspond to 1:1 and 2:3 slopes. Figure 7 shows that the ratio between the vertical and horizontal components tends to be larger than unity as depth decreases. Figures 6 and 7 give us a clear and direct picture of the site effects on the recorded ground motions. The deamplification of horizontal motions, as mentioned previously, is believed to be caused by the liquefaction in shallow layers, which was associated with substantial softening of soils. Abundant evidence of site liquefaction such as sand boils, ground fissures, and lateral spreading of as much as 5.9 m was observed after the earthquake (Shibata et al. 1996; Hamada et al. 1996). The significant vertical amplification, on the other hand, is considered

Fig. 4. Vertical array acceleration records at Port Island during the 1995 Kobe earthquake. EW, east–west; NS, north–south.

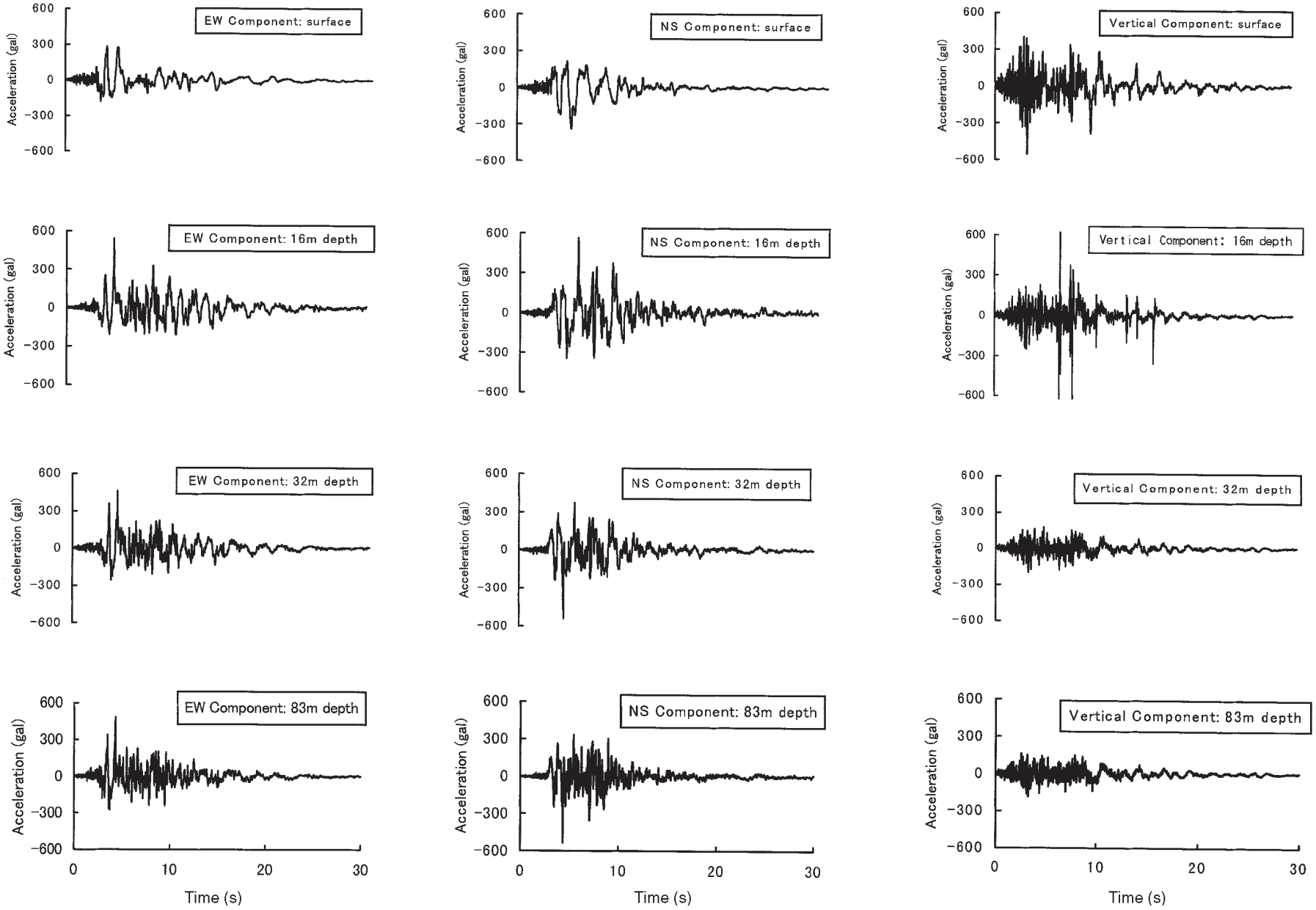

Fig. 5. Displacement orbits at four stations at different depths. EW, east–west; NS, north–south.

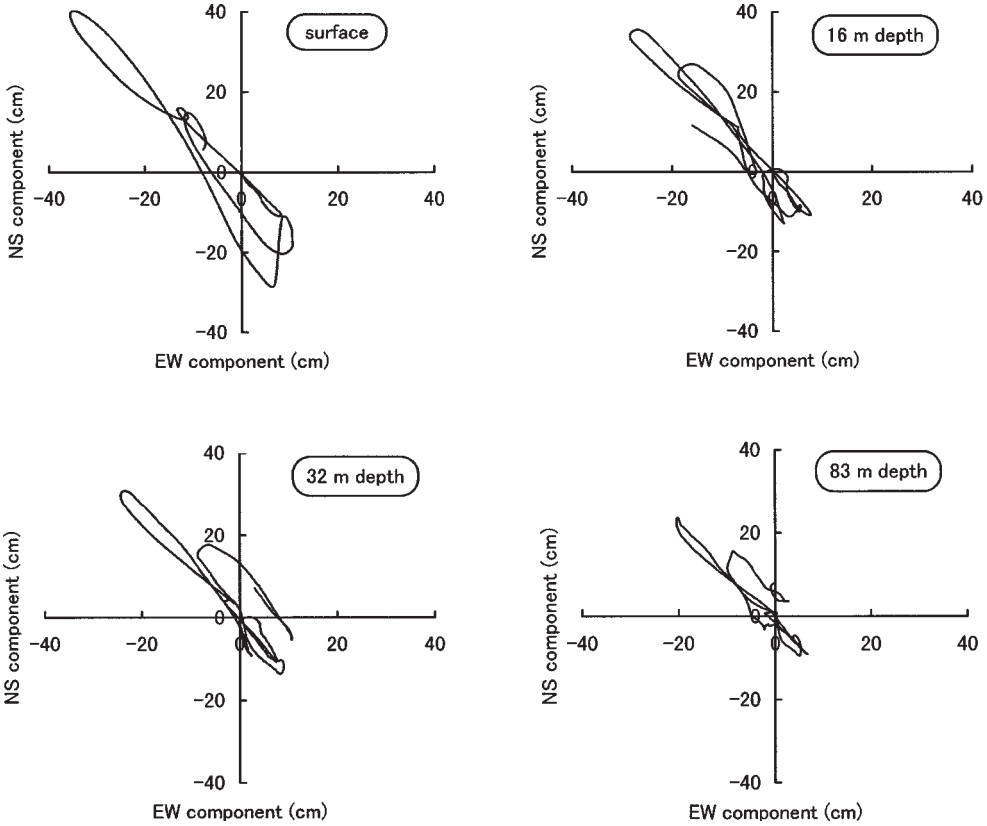

Fig. 6. Distribution of maximum horizontal accelerations with depth. EW, east–west; NS, north–south.

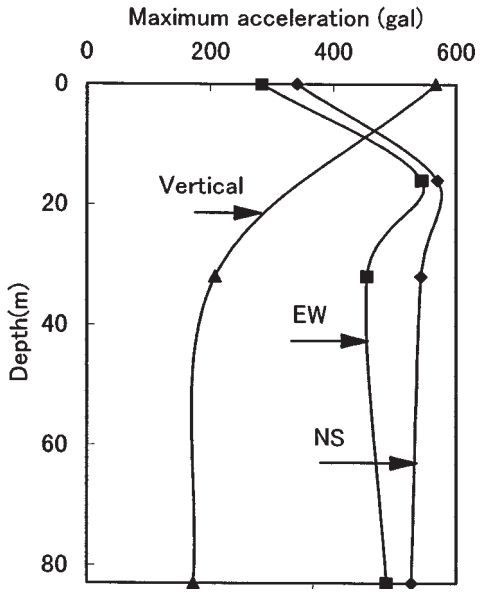

Fig. 7. Relationship of maximum horizontal and vertical accelerations at different depths. EW, east–west; NS, north–south.

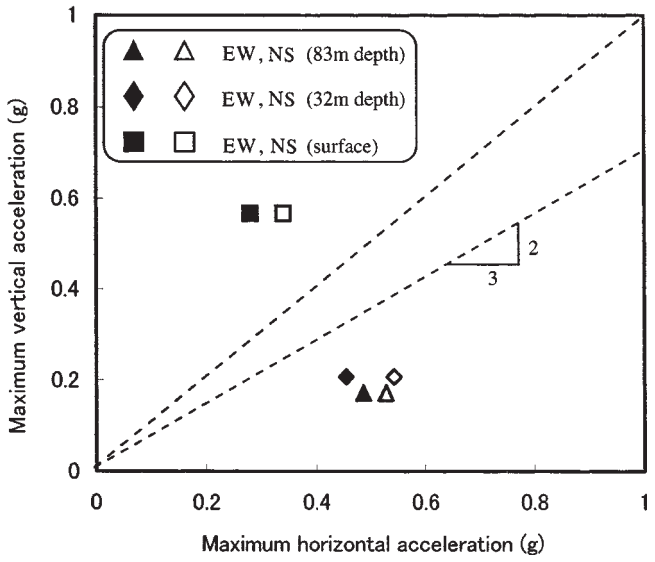

as the result of incomplete saturation of near-surface soils which caused substantial amplification of P waves because the vertical motion may mainly involve the propagation of P waves (Yang and Sato 2000*a*). A detailed discussion on this issue is of interest but beyond the scope of the present paper. The relevant studies are presented in Yang and Sato (2000*a*, *b*).

Spectral analysis of ground motion

Subsurface soils subjected to a strong shaking may respond in a nonlinear manner. As a result, the amplitude of horizontal motion may be reduced and the predominant period of the motion lengthened. In general, this nonlinear response can be investigated by examining the Fourier response or spectral ratio between the surface motion and

Fig. 8. Fourier spectra of horizontal surface motions in three phases: (*a*) north–south component, and (*b*) east–west component.

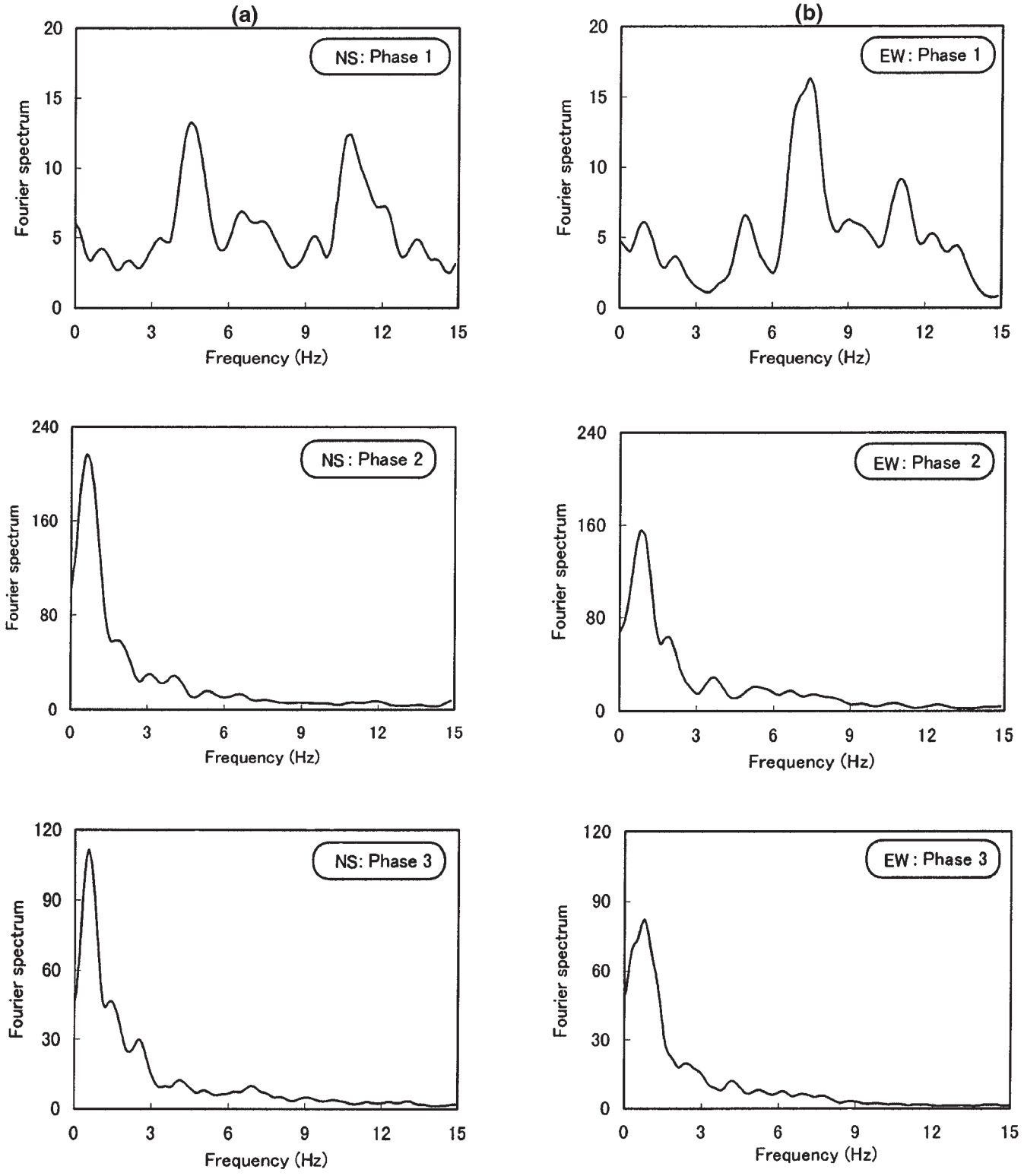

the motion recorded at other depths. However, because of the long duration of the acceleration records and uncustomary variation of the frequency content, it is difficult to reach a reliable conclusion from the spectral analysis of the complete records. An approach to deal with this problem is to divide the long records into several phases so as to capture the variation of frequency content during the shaking. In this study, each acceleration record is separated into three phases according to the observed features of seismograms: phase 1, from 0 to 3 s, contains weak earthquake motions with maximum acceleration less than 100 gal; phase 2, from 3 to 12 s, corresponds to the strongest motions with maximum acceler-

Fig. 9. Spectral ratios for three phases for the north–south component of ground motion.

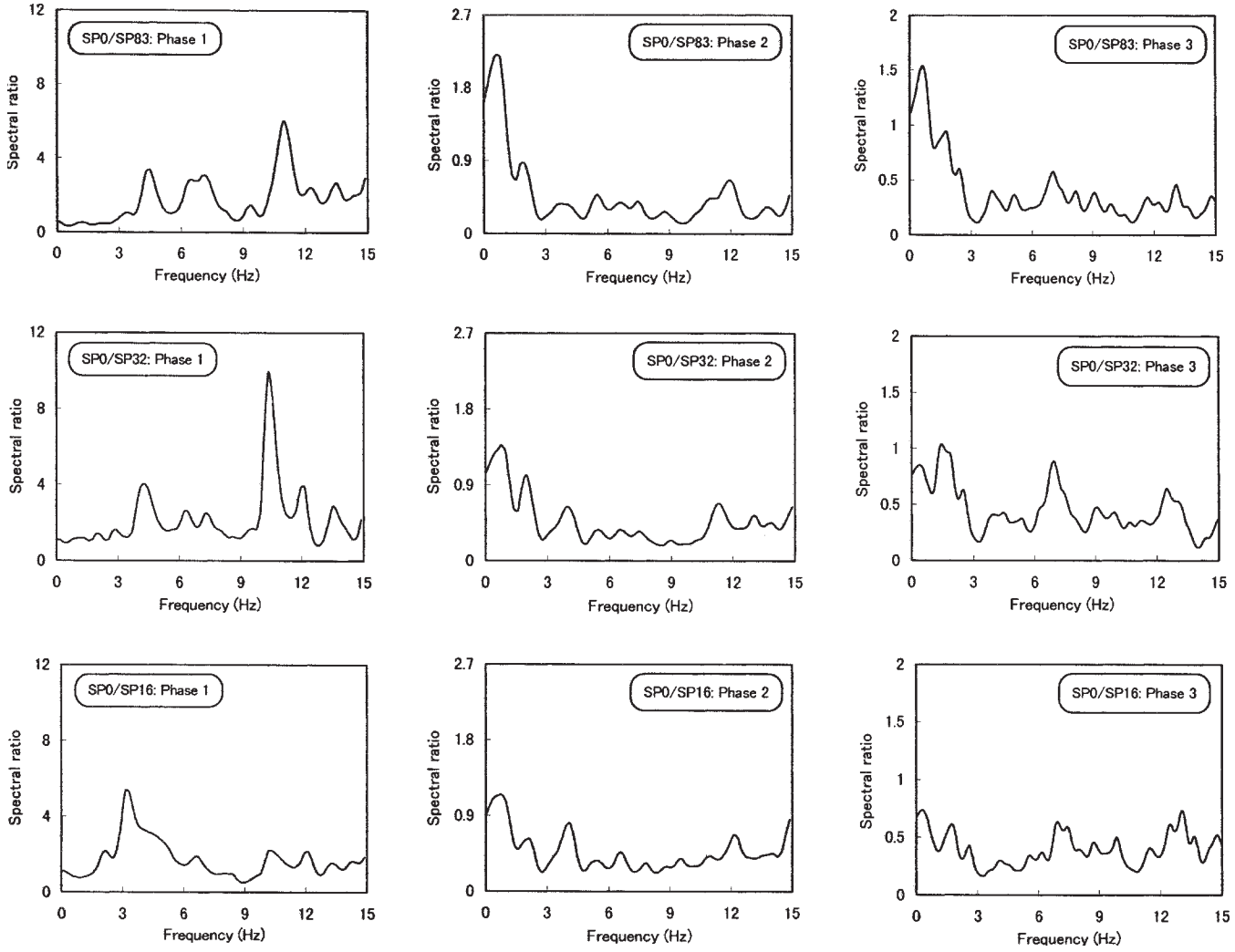

ation around 560 gal; phase 3, from 12 to 30 s, contains weak motions after the strong motions.

The Fourier spectra for the surface motion in two horizontal directions are investigated. In the calculation of the Fourier spectra for the three phases, a smoothing of the spectra is performed using Parzen's spectral window (Bellanger 1989). Figures 8*a* and 8*b* show the spectral amplitudes for the surface motions for three phases in the north–south and east–west directions, respectively. As expected, the predominant frequencies for both horizontal motions were decreased when the strong motion occurred. For the north–south direction, the predominant frequencies dropped from about 4.5 and 10.8 Hz in phase 1 to 0.6 Hz in phase 2; for the east–west direction, the predominant frequencies decreased from about 4.8 and 7.5 Hz in phase 1 to 1 Hz in phase 2. The decrease in predominant frequency was associated with the strong earthquake shaking, which caused soil softening and liquefaction in shallow layers. Moreover, the frequency content of the surface motion in phase 2 is similar to that in phase 3, which may indicate that the liquefaction state of soils remained within the period.

The spectral ratios between the motions recorded at the surface and other stations were analyzed and provide a good representation of the transfer functions for different locations. Figures 9*a*, 9*b*, and 9*c* show the spectral ratios between the surface motion and the motions at depths of 16, 32, and 83 m (denoted SP0/SP16, SP0/SP32, and SP0/SP83) in three phases, respectively, for the north–south direction. The spectral ratios in three phases for the east–west direction are shown in Fig. 10. Generally, the features of the spectral ratios for the east–west component are very similar to those for the north–south component for all three phases. Therefore, the discussion of the characteristics of spectral ratios is focused here on the north–south component. From the plots in Fig. 9 it can be seen that, in phase 1, the spectral ratios SP0/SP83 and SP0/SP32 are similar, with peak frequencies of around 4.5, 7.0, and 11.0 Hz and 4.2, 6.0, 10.5 Hz, respectively. The dominant seismic waves were those with high frequencies in this phase. However, the spectral ratio SP0/SP16 exhibited a slightly different feature: the peak frequencies were around 3.2 and 6.6 Hz. This indicates that, although the shaking during this stage was not strong, seismic motions with relatively longer periods became dominant when the waves travelled through the surface reclaimed layer. Such an influence of different soil layers on the ground motions was also well manifested in surface motion records, as shown in Fig. 8: two predominant frequencies, around 4.5 and 11 Hz, were

Fig. 10. Spectral ratios for three phases for the east–west component of ground motion.

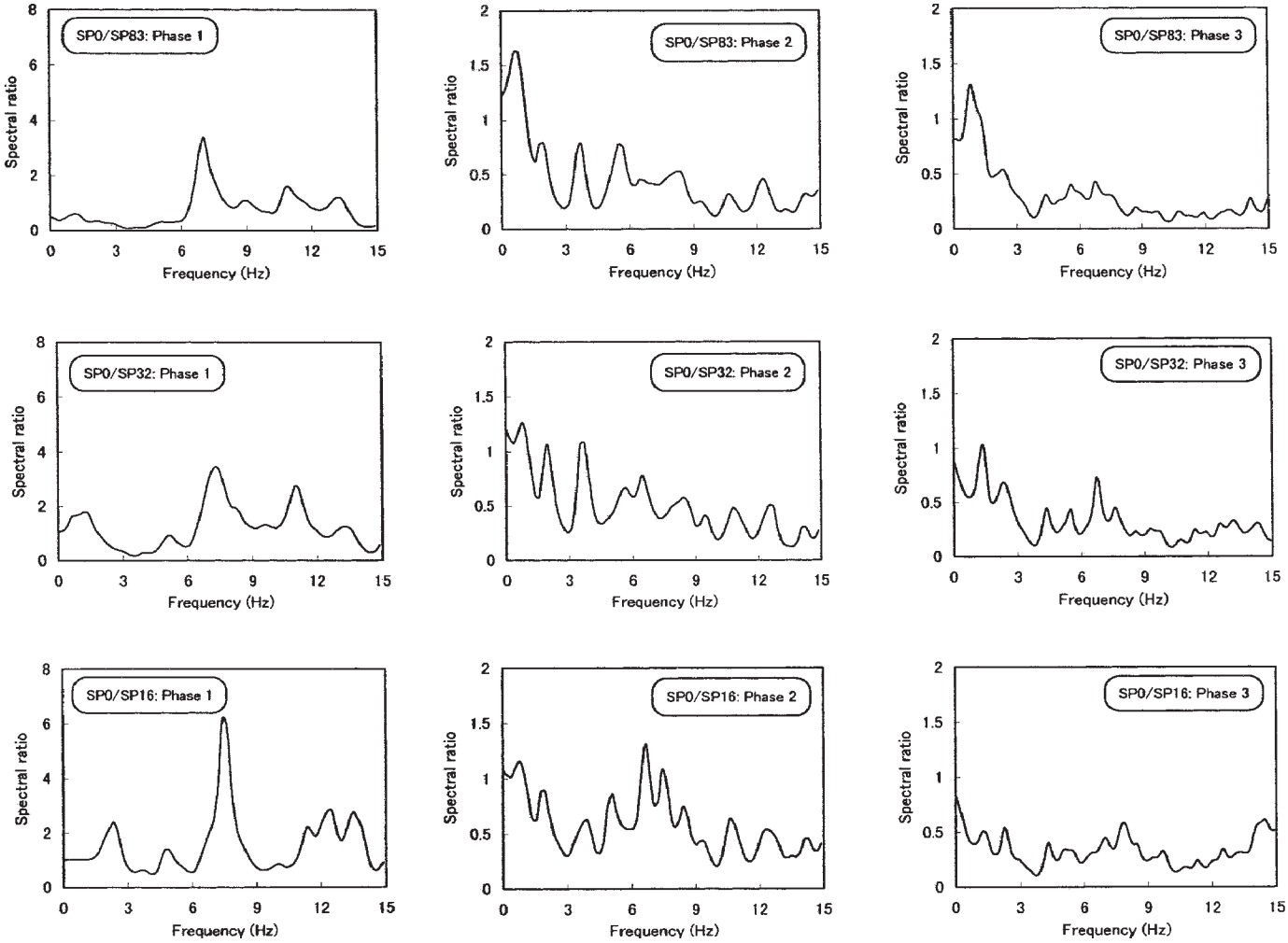

observed in the spectra of surface motion in phase 1. On the other hand, by comparing the spectral ratios in phases 1 and 2, the influence of nonlinear soil behavior, which was attributed to a strong shaking, was clearly observed: the frequency contents were obviously shifted to the low-frequency end, in other words, the predominant periods were lengthened when the strong motion occurred. In phase 2 the amplitudes for the waves with frequencies higher than 5 Hz were dramatically reduced, with amplification ratios below 1, whereas in phase 1 these waves were amplified notably. The difference for the two phases indicates that the increase in the predominant period was caused primarily by a strong decrease in the amplitude of low-period waves, rather than by amplification of long-period motion. Similarly, the spectral ratios for phase 3 are generally similar to those in phase 2.

Identification of nonlinearity in liquefied reclaimed layer

As shown earlier in the paper, the surface reclaimed layer has a significant influence on the surface ground motion. This layer consisted of decomposed granite which has a high liquefaction susceptibility. The spectral analysis of the recorded motions indicated that significant soil softening occurred in this layer during the strong shaking. It is possible to back-calculate the change in soil stiffness during the earthquake from the field records. The method used here is based on wave propagation in a layered system, as shown in Fig. 11. For this simplified model, the transfer function is given as

Fig. 11. Seismic wave propagation in a layered system.

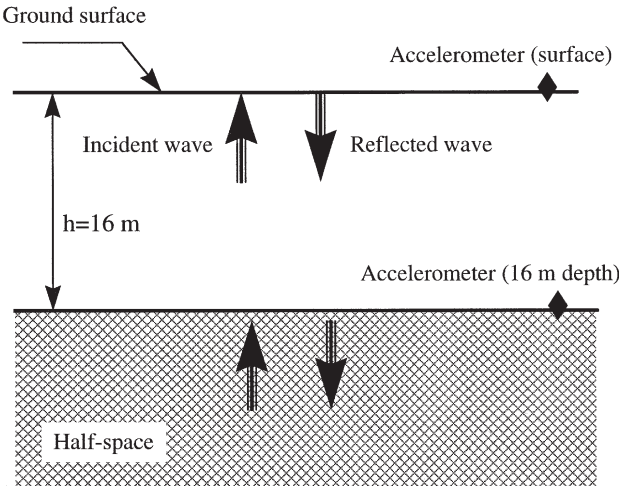

Table 1. Identified shear wave velocity and shear modulus for the surface reclaimed layer.

Component	f_1, phase 1 (Hz)	f_2, phase 2 (Hz)	V_{s1}, phase 1 (m/s)	V_{s2}, phase 2 (m/s)	G_1, phase 1 (MPa)	G_2, phase 2 (MPa)	Reduction of G $(G_1 - G_2)/G_1$ (%)
North–south	3.2	0.8	205	51	79.8	4.9	94
East–west	2.4	0.89	154	57	45.1	6.2	86

Note: PS logging: V_s = 198 m/s and G_0 = 74.5 MPa (average values for the reclaimed layer, G.L. 0 to –16 m).

Fig. 12. Undrained response of soil model calibrating from cyclic strength data.

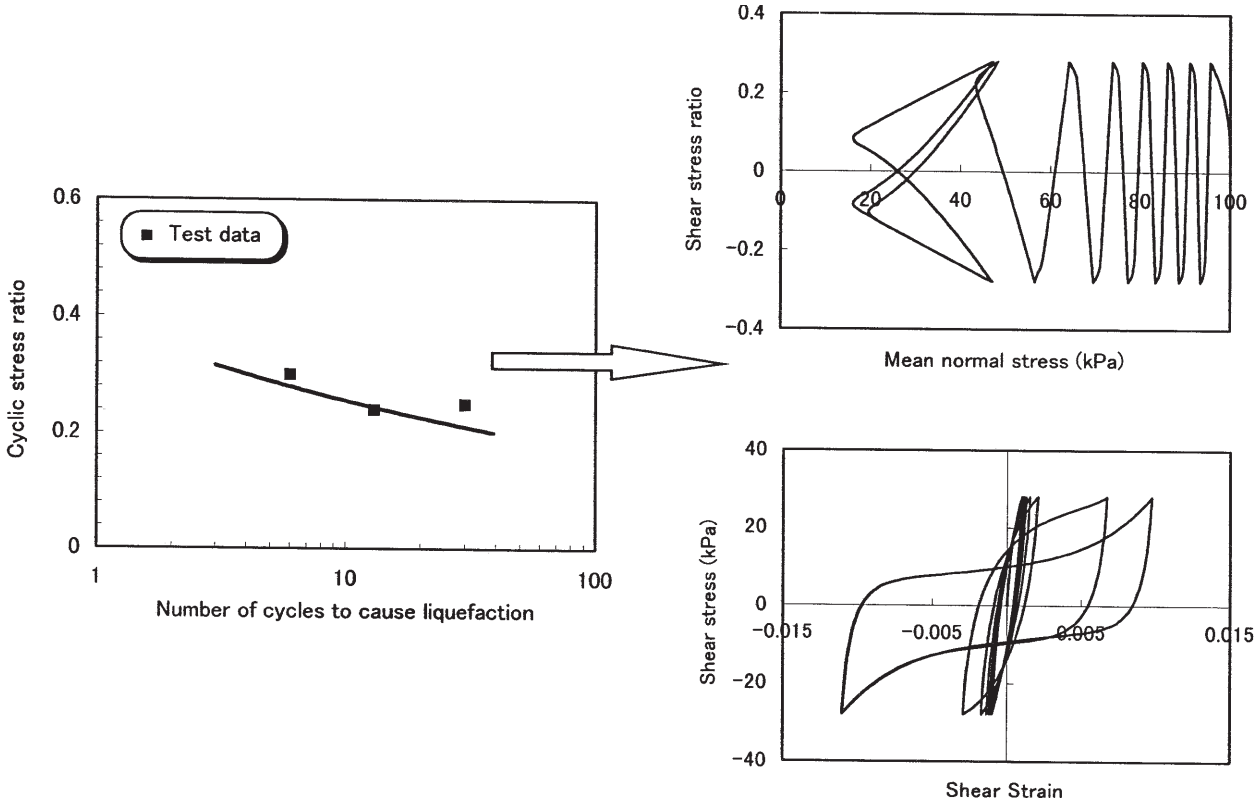

$$[1] \qquad T(f) = \left(\cos \frac{2\pi f h}{V_s} \right)^{-1}$$

where V_s is the shear-wave velocity of the layer, h is the thickness of the layer, and f is the frequency. With the identified fundamental frequency and eq. [1], the shear-wave velocity and shear modulus for the liquefied layer (from the surface to a depth of 16 m) are calculated for the two phases for the north–south and east–west components as shown in Table 1. These values correspond, respectively, to the average soil stiffness before and after the strongest earthquake shaking. For example, the average shear modulus identified in the north–south component is about 79.8 MPa before the strongest shaking, and it dropped to 4.9 MPa after the strongest shaking. The reduction of shear modulus during the shaking event is remarkable: it is about 94% for the north–south component and 86% for the east–west component. It should be mentioned that the shear modulus after the strongest shaking shown above is not the exact stiffness for liquefied soil but some equivalent modulus of combined liquefied and nonliquefied soils.

Nonlinear analysis of ground response of array site

In this section, a coupled nonlinear finite element analysis of the site response to the recorded motions is described. The purpose is to compute the acceleration time histories, pore-water pressure responses, and stress–strain histories of soils at different depths and then to examine their relations to the observed characteristics of ground motions. This would provide a better understanding of the nonlinear soil behavior and its influence on ground motions.

The numerical procedure applied is a fully coupled effective-stress procedure for site response under multidirectional earthquake shaking (Li et al. 1998), which is formulated based on Biot's theory of two-phase media (Biot 1941, 1962; Zienkiewicz and Shiomi 1984). The basic assumptions made in the formulation are as follows: (1) the site is horizontally layered and extends infinitely in horizontal directions, (2) the ground surface is free of stresses and the bottom boundary is impermeable, (3) soil below the water table is saturated and the water flow obeys Darcy's law, and

Fig. 13. Simulated and recorded acceleration–time histories at different depths.

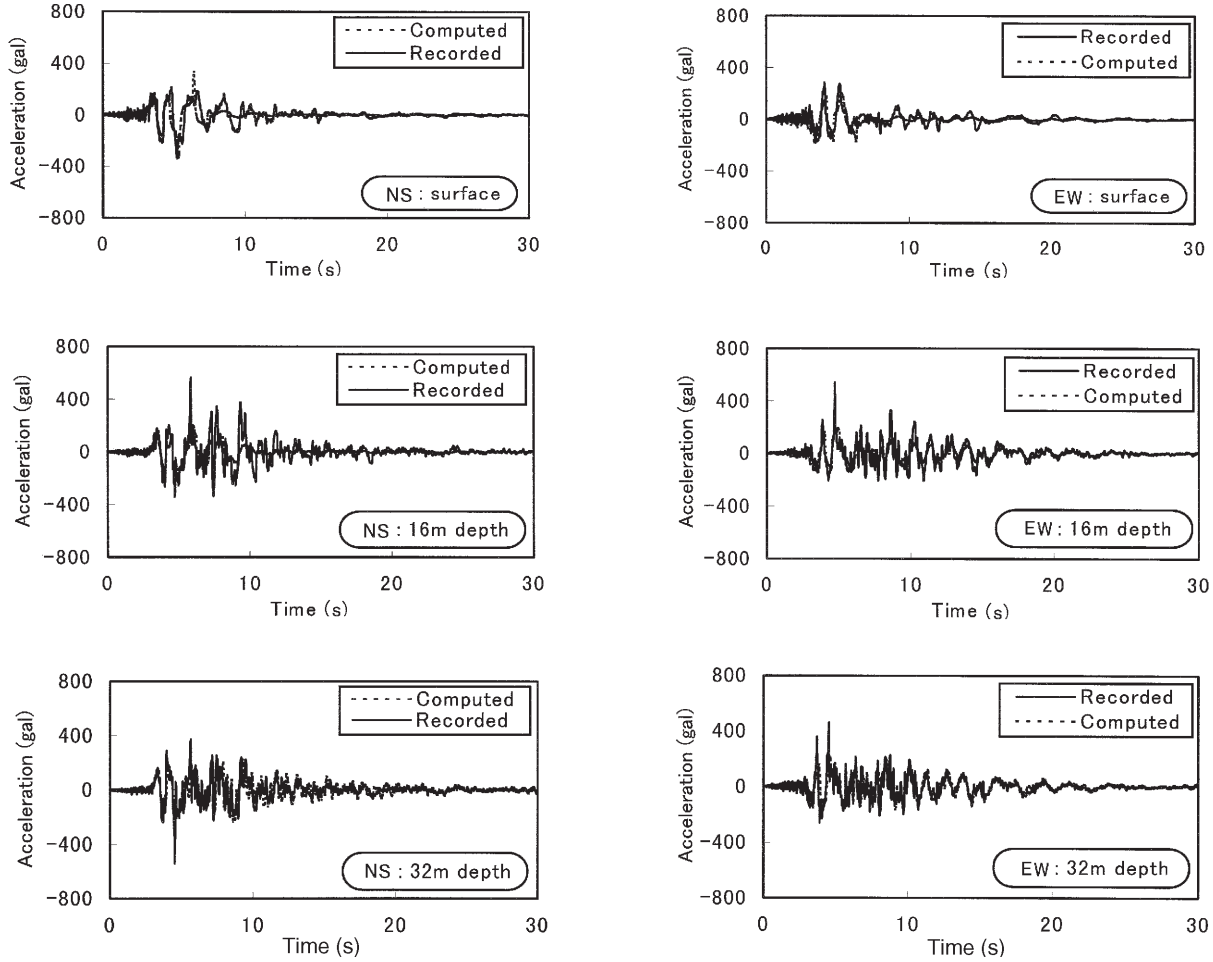

(4) seismic waves travel along the vertical direction only. These assumptions, in practice, conform to free-field soil deposits that are water saturated, essentially levelled, and subjected to earthquake shaking originating primarily from the underlying rock formation.

The inelastic soil model incorporated in the procedure is a hypoplasticity bounding surface model (Wang et al. 1990) which was developed within the framework of bounding surface theory (Dafalias 1986). The model is capable of realistically simulating the soil behavior under a wide range of loading conditions, such as the compression- and dilation-induced effective stress change, the lateral stress change due to shaking, and the significant reduction of stiffness upon liquefaction. For level ground earthquake response problems, the model takes a reduced-order form and has 10 model parameters to be determined for a particular soil. The parameters are described as follows: (1) a coefficient G_0 defining elastic shear modulus using the following equation:

$$G_{\max} = G_0 \frac{(2.973 - e_0)^2}{1 + e_0} \sqrt{p p_{\text{atm}}}$$

where e_0 is the initial void ratio, p is the effective mean normal stress, and p_{atm} is atmospheric pressure; (2) the slope λ of the virgin compression line; (3) the slope κ of the rebounded line which is defined as

$$\kappa = \frac{3(1 + e_0)^2(1 - 2\nu)}{2G_0(2.973 - e_0)^2(1 + \nu)}$$

where ν is Poisson's ratio; (4) the slope R_f of the failure line; (5) the slope R_p of the phase-transformation line; (6) the term h_r, which characterizes the relationship between shear modulus and shear strain magnitude; (7) the term d, which characterizes the rate of effective mean normal stress change caused by shear unloading; (8) the term k_r, which characterizes the amount of effective mean normal stress change caused by shear loading; (9) b, a parameter affecting the shape of the stress paths of the virgin shear loading; and (10) h_p, a parameter controlling the amount of the shear strain increment due to the change of the maximum effective mean normal stress. Among these parameters, λ and h_p are active only when the mean normal stress exceeds its maximum value in the loading history. During earthquakes the mean normal stress in soil is almost always less than its initial value, thus the two parameters are inactive for ground response analyses. The parameter b is also inactive in the calculation, with a typical value of 2. The remaining parameters should be calibrated specifically for a given soil either by laboratory tests or from field data. In Fig. 12 the response of the soil model to cyclic loading calibrated on the basis of the liquefaction-resistance data for reclaimed soils is presented. The corresponding model parameters are given in

Table 2. Model parameters for reclaimed soils (sublayer 2).

Parameter	Value
G_0	250.7
λ	0.006
κ	0.0011
R_f	0.85
R_p	0.76
h_r	0.386
d	5.0
k_r	0.4
b	2
h_p	35

Table 2. A complete discussion on the constitutive model and the parameter calibration is beyond the scope of this paper. The reader is referred to Wang et al. (1990) and Dafalias (1986) for details.

The bottom boundary of soil deposits can be treated as a rigid base if the input motions are taken directly from downhole records. When the input motions are specified at outcropping rock, the underlying base can be approximately regarded as an uniform elastic half-space characterized by its mass density and wave velocities, and the boundary conditions can be established based on the theory of elastic wave propagation. The present analysis is for the top 83 m of the deposit and the acceleration records at this depth serve as input motions.

The calculated and recorded acceleration time histories at the surface and depths of 16 and 32 m in the north–south and east–west directions are shown in Fig. 13. The calculated and recorded ground surface acceleration response spectra are shown in Fig. 14. In general**,** the calculated acceleration histories are very similar to the field records. The discrepancy between the calculations and records is considered acceptable, considering the strong input motions and the uncertainties involved in the analyses. Obviously, the motions were deamplified both in the north–south and east–west components when the seismic waves were travelling from the bottom to the top. The computed stress–strain histories at depths of 7.7, 24, and 51.3 m during the shaking are shown in. Figs. 15*a* and 15*b* for the north–south and east–west directions, respectively. Here, the shear stress is normalized to the initial effective vertical stress. The soils at different depths exhibited quite different behavior during the earthquake in either direction. The soils at the shallow depth (7.7 m) showed a dramatic reduction of soil stiffness. In particular, the shear modulus of soils was reduced almost to zero while the shear strain remained at a high level at the final stage of strong shaking, indicating that the soils liquefied fully. On the other hand, soils at the deeper depth (51.3 m) responded in a small nonlinear manner, with no appreciable reduction of stiffness and with a low level of strain. The stress–strain history for the soils at a depth of 24 m indicates a moderate reduction of shear modulus, but the soils did not fully lose strength throughout the earthquake. The calculated strain levels for the soils at the three different depths are in good agreement with the evaluations by Kazama et al. (1996), in which the stress–strain relationships were directly

Fig. 14. Ground surface acceleration response spectra. EW, east–west; NS, north–south.

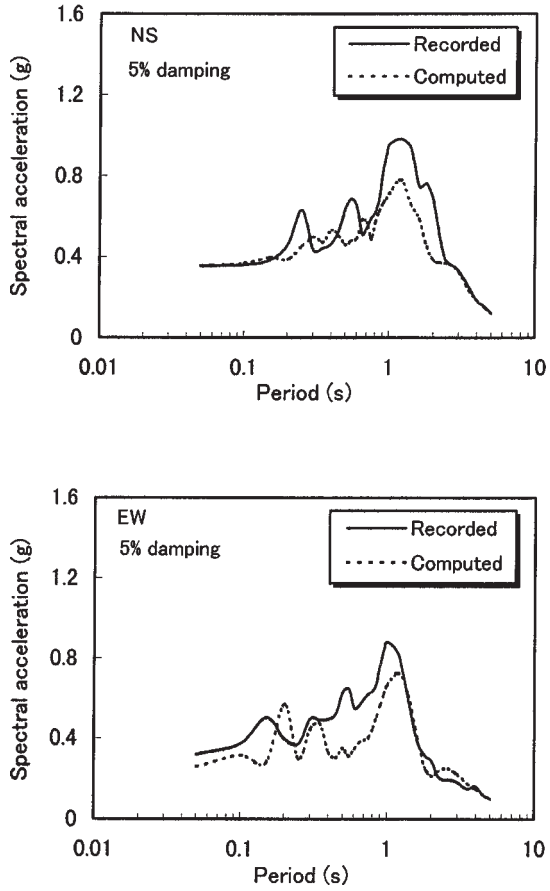

calculated from downhole records using the integration technique. According to their study the maximum strain is around 1–2% for the reclaimed soils between the surface and a depth of 16 m, around 0.6% for the soils between depths of 16 and 32 m, and around 0.1–0.2% for the soils between depths of 32 and 83 m.

Figure 16 depicts the excess pore-water pressure responses at depths of 7.7 and 51.3 m during the shaking. The pore pressure is normalized with the corresponding initial effective vertical stress. Figure 16 shows that an abrupt rise in excess pore-water pressure occurred during the phase of strongest excitation (phase 2, 5–8 s). For the soils at a depth of 7.7 m, the excess pore pressure reached the value of initial effective vertical stress at around 8 s, which resulted in a full soil liquefaction. Corresponding to this stage, the soil stiffness was reduced significantly, and consequently the frequency content of surface motion was decreased notably, as shown in Fig. 8.

Figure 17 shows the relation of ground motion and soil behavior during the earthquake. The recorded surface motion in the north–south component, and its Fourier spectra in the three phases, and the stress–strain histories of soils at a depth of 7.7 m at different stages are shown. It is obvious that in the first phase, which corresponds to weak shaking, the soil responded almost linearly with the strain level of the order of 0.01%, the typical threshold strain for sand (Dobry et al. 1982); the generated excess pore-water

Fig. 15. Calculated stress–strain histories of soils at different depths: (*a*) north–south component, and (*b*) east–west component.

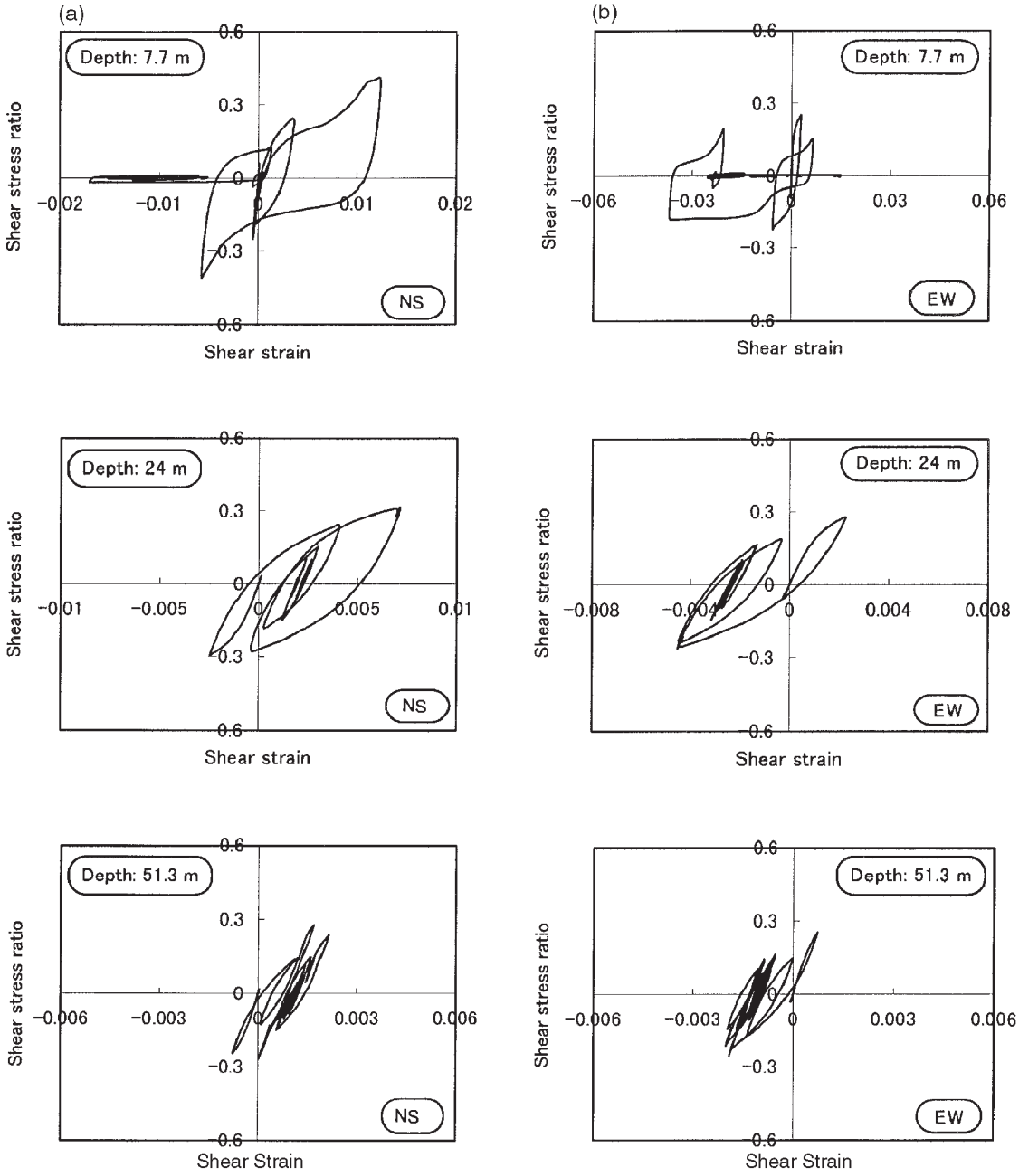

pressure at this stage was very small, as shown in Fig. 16. Corresponding to this stage, the spectra of the surface motion were dominated by high-frequency components (with peak frequencies of 4.5 and 10.8 Hz). During the stage from 3 to 6 s, which corresponds to the strong shaking, the soil exhibited an obvious nonlinearity, with the peak strain of the order of 1%. The generated excess pore pressure reached 75% of the initial effective vertical stress at 6 s. Although full liquefaction was not triggered at this stage, the nonlinearity was sufficiently large to cause an obvious influence on the acceleration records. During the period from 6 to 12 s, the abrupt loss of soil stiffness upon liquefaction was clearly observed. The amplitude of shear strain approximately reached the value of 2%. Correspondingly, the long-period waves were dominant in surface motion (with a peak frequency of 0.6 Hz).

Conclusions

In this paper, nonlinear site effects were studied using the case history of a reclaimed site subjected to the 1995 Kobe earthquake. The characteristics of the downhole array acceleration records were analyzed and a coupled inelastic finite element simulation of the site response was carried out. The present study indicates the following:

(1) The difference in the characteristics of ground motions before and after the strongest earthquake shaking is large.

Fig. 16. Calculated excess pore-water pressure responses at different depths.

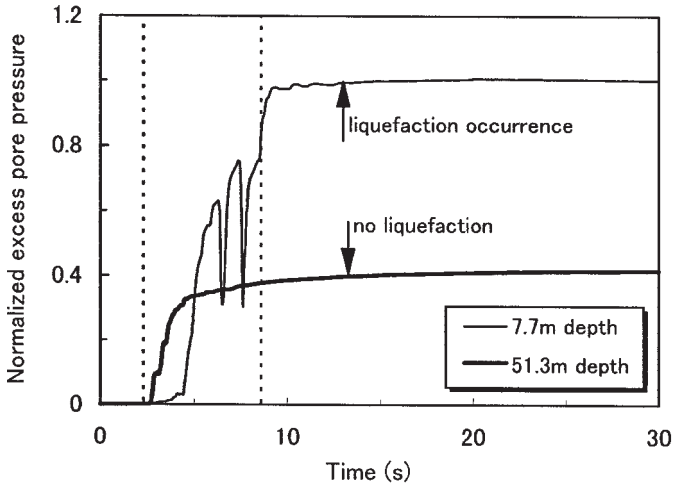

The peak frequencies in spectral ratios were shifted to lower frequencies when the strongest motions occurred.

(2) The increase in the predominant period of seismic motion was caused primarily by the attenuation of low-period waves, rather than by amplification of long-period motions.

(3) The influence of soil behavior on ground motion was different for different soil layers, which is manifested in the spectral ratios. The surface reclaimed soils played a key role in modifying the characteristics of ground motions.

(4) The identified shear modulus using spectral ratios showed a significant variation in the behavior of surface soils before and after the strongest shaking. The reduction of shear modulus was 94% in the north–south component and 86% in the east–west component, implying that this layer may have fully liquefied during the earthquake.

(5) The simulated stress–strain histories and excess pore-water pressure response were well correlated with the variation of the characteristics of ground motions. Corresponding to the initial weak motion stage, the shallow soil responded linearly and the ground motion was dominated by high-

Fig. 17. Relation of soil behavior and ground motion during earthquake shaking.

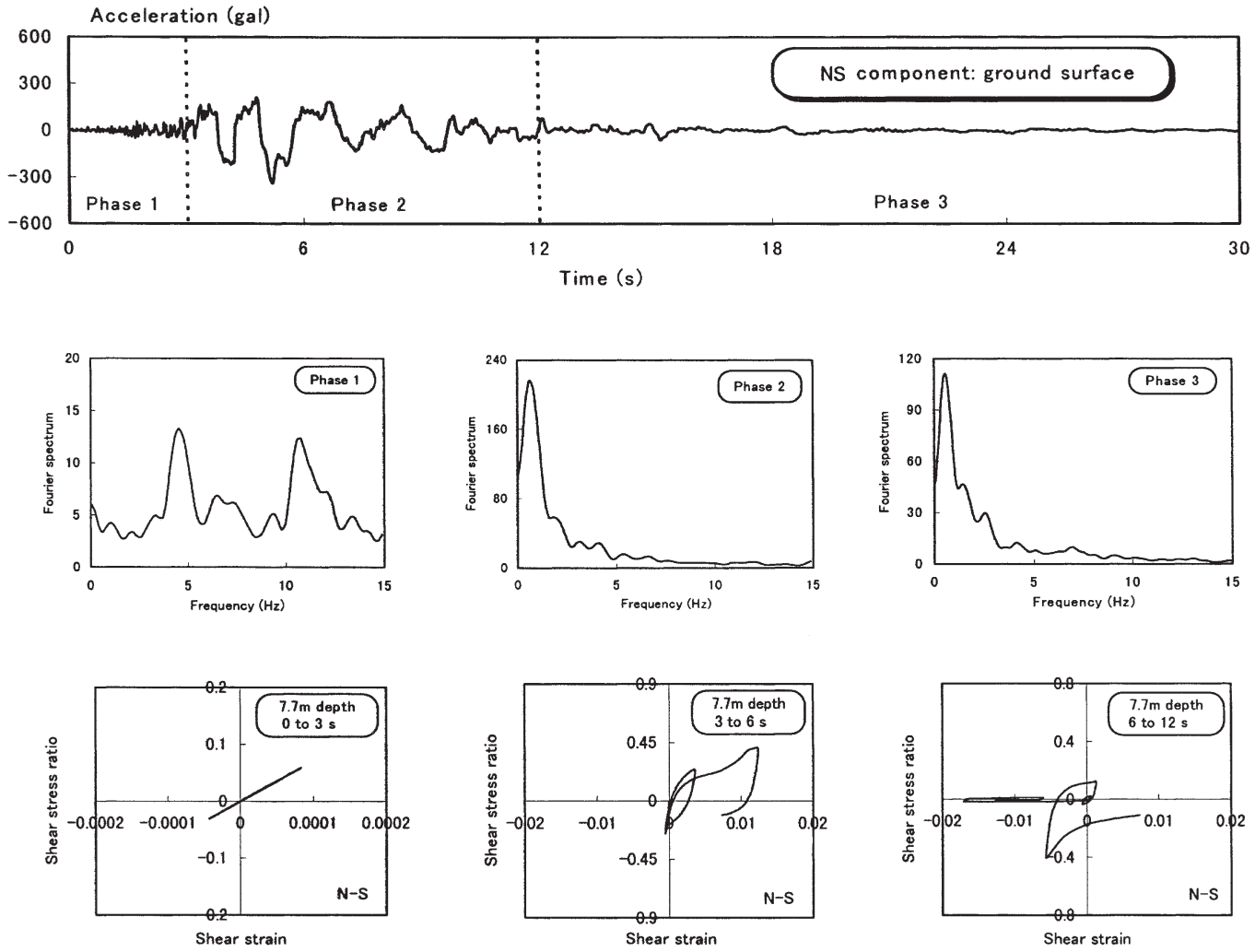

frequency waves. When the strongest shaking occurred, the soil performed nonlinearly and an abrupt loss of stiffness took place upon liquefaction. Correspondingly, the surface motion was dominated by long-period waves.

Acknowledgments

The first author would like to acknowledge the financial support provided by the Ministry of Education and Science, Japan, via the program of Center of Excellence and the support by the Japan Society of Civil Engineers via STA project. The downhole acceleration data and soil profile for the array site were provided by the Kobe City Development Bureau, Japan. The authors also wish to thank the anonymous reviewers for their valuable comments and suggestions.

References

Bellanger, M. 1989. Digital processing of signals: theory and practice. Wiley, Chichester, U.K.

Beresnev, I.A., Wen, K.L., and Yeh, Y.T. 1995. Seismological evidence for nonlinear elastic ground behavior during large earthquakes. Soil Dynamics and Earthquake Engineering, **14**: 103–114.

Biot, M.A. 1941. General theory of three-dimensional consolidation. Journal of Applied Physics, **12**: 155–164.

Biot, M.A. 1962. The mechanics of deformation and acoustic propagation in porous media. Journal of Applied Physics, **33**: 1482–1498.

Chang, C.Y., Mok, C.M., Power, M.S., Tang, Y.K., Tang, H.T., and Stepp, J.C. 1991. Development of shear modulus reduction curves based on Lotung downhole data. *In* Proceedings of the 2nd International Conference on Recent Advances in Geotechnical Earthquake Engineering and Soil Dynamics, Rolla, Mo., pp. 111–118.

Dafalias, Y.F. 1986. Bounding surface plasticity, I. Mathematical foundation and the concept of hypoplasticity. Journal of Engineering Mechanics, ASCE, **112**: 966–987.

Dobry, R., Ladd, R.S., Yokel, F.Y., Chung, R.M., and Powell, D. 1982. Prediction of pore water pressure buildup and liquefaction of sands during earthquakes by the cyclic strain method. NBS Building Science Series (United States), No. 138.

Elgamal, A.W., Zeghal, M., Tang, H.T., and Stepp, J.C. 1995. Lotung downhole array, II: evaluation of site dynamic properties. Journal of Geotechnical Engineering, ASCE, **121**: 363–378.

Hamada, M., Isoyama, R., and Wakamatsu, K. 1996. Liquefaction-induced ground displacement and its related damage to lifeline facilities. Soils and Foundations, Special Issue No. 1, pp. 81–97.

Hardin, B.O., and Drnevich, V.P. 1972. Shear modulus and damping in soil: measurement and parameter effects. Journal of the Soil Mechanics and Foundations Division, ASCE, **98**: 603–624.

Ishihara, K. 1993. Liquefaction and flow failure during earthquakes. Géotechnique, **43**: 351–415.

Kazama, M., Yanagisawa, E., Inatomi, T, Sugano, T., and Inagaki, H. 1996. Stress strain relationship in the ground at Kobe Port Island during 1995 Hyogoken–Nambu earthquake inferred from strong motion array records. Proceedings of the Japan Society of Civil Engineers, No. 547/III-36, pp. 171–182.

Kobe City Development Bureau. 1995. A report on the investigations on the deformation of the reclaimed site during the 1995 Hyogoken–Nambu earthquake. Kobe City Development Bureau, Kobe, Japan.

Kokusho, T. 1980. Cyclic triaxial test of dynamic soil properties for wide strain range. Soils and Foundations, **20**: 45–60.

Li, X.S., Shen, C.K., and Wang, Z.L. 1998. Fully coupled inelastic site response analysis for 1986 Lotung earthquake. Journal of Geotechnical and Geoenvironmental Engineering, ASCE, **124**: 560–573.

Nagase, H., Shinji, R., Kimura, K., and Tsujino, S. 1995. Liquefaction strength of undisturbed sand subjected to overconsolidation. *In* Proceedings of the 30th Japan National Conference on Geotechnical Engineering. Kanazawa, Japan (In Japanese.)

NRC. 1985. Liquefaction of soils during earthquakes. National Research Council (NRC) Report CETS-EE-0001.

Seed, H.B. 1979. Soil liquefaction and cyclic mobility evaluation for level ground during earthquakes. Journal of the Geotechnical Engineering Division, ASCE, **105**: 201–255.

Seed, H.B., and Idriss, I.M. 1970. Soil moduli and damping factors for dynamic response analysis. Report EERC 70-10, Earthquake Engineering Research Center, University of California, Berkeley, Calif.

Shibata, T., Oka, F., and Ozawa, Y. 1996. Characteristics of ground deformation due to liquefaction. Soils and Foundations, Special Issue No. 1, pp. 65–79.

Sugito, M., and Kamada, H. 1990. Nonlinear soil amplification model with verification by vertical strong motion array records. *In* Proceedings of the 4th U.S. National Conference on Earthquake Engineering, Irvine, U.S.A. pp. 555–564.

Sugito, M., Sekiguchi, K., Yashima, A., Oka, F., Taguchi, Y., and Kato, Y. 1996. Correction of orientation error of borehole strong motion array records during the South Hyogo Earthquake of Jan. 17, 1995. Proceedings of the Japan Society of Civil Engineers, No. 531/I-34, pp. 51–63.

Vucetic, M., and Dobry, R. 1991. Effect of soil plasticity on cyclic response. Journal of Geotechnical Engineering, ASCE, **117**: 89–107.

Wang, Z.L., Dafalias, Y.F., and Shen, C.K. 1990. Bounding surface hypo-plasticity model for sand. Journal of Engineering Mechanics, ASCE, **116**: 983–1001.

Yang, J., and Sato, T. 2000*a*. Interpretation of seismic vertical amplification observed at an array site. Bulletin of the Seismological Society of America, **90**: In press.

Yang, J., and Sato, T. 2000*b*. Characterization of a reclaimed site and its seismic vertical amplification. Geotechnical Special Publication (Geo-Denver 2000), ASCE.

Zienkiewicz, O.C., and Shiomi, T. 1984. Dynamic behaviour of saturated porous media: the generalized Biot formulation and its numerical solution. International Journal of Numerical and Analytical Methods in Geomechanics, **8**: 71–96.